Hybrid cooperative positioning for vehicular networks

Author:

Xiong, J; Cheong, JW; Xiong, Z; Dempster, AG; Tian, S; Wang, R

Hybrid Cooperative Positioning for Vehicular Networks

Jun Xiong , Joon Wayn Cheong , *Member, IEEE*, Zhi Xiong, Andrew G. Dempster , *Senior Member, IEEE*, Shiwei Tian , and Rong Wang

Abstract—This paper proposes a hybrid cooperative positioning (CP) algorithm suitable for vehicular network applications which can fuse the measurements from global navigation satellites, ground stations, signals of opportunity, inter-node ranging from neighbouring vehicles and onboard inertial navigation systems (INS). By applying the framework of generalized approximate message passing (GAMP), the complex CP problem is transformed into an iterative yet lower computational load process. In each iteration, the time recurrence of navigation states and initialization of GAMP computation are conducted based on Kalman filter. The proposed algorithm guarantees the overall positioning performance of multiple vehicles in a hybrid navigation scenario, and improves the robustness and accuracy of CP navigation systems. Simulation results show that the proposed algorithm has better estimation accuracy than traditional CP algorithms, and has 20 times less computational load than the best existing algorithm with equivalent accuracy.

Index Terms—Approximate message passing, Cooperative positioning, Kalman filter, Vehicular networks.

I. INTRODUCTION

POSITIONING is a fundamental issue for vehicles. To guarantee the safety and efficiency of systems, many applications such as intelligent transportation systems (ITS) [1], location-based services (LBS) [2] and automatic drive [3] are very dependent on accurate navigation solutions. However, for a classical vehicle onboard navigation system, most are integrated navigation systems based on global navigation satellite system (GNSS) and inertial navigation systems (INS). The main defect of this navigation scheme is that the positioning performance largely depends on the GNSS for correcting its drift errors. If the number of available satellites is not enough for positioning calculation, it is difficult to maintain a reliable and durable positioning solution. To deal with this problem, one effective approach is to enhance the positioning accuracy using a fixed known positioning base station, such as the Real Time Kinematic (RTK) technique. However, this method needs large numbers of expensive base stations to guarantee system continuity. Another way is to equip external navigation sensors such as millimeter-wave radar, camera, or Lidar to augment the navigation system. However for most vehicle applications, it is rare to carry large numbers of navigation sensors due to restricted working scenarios and cost constrains.

Therefore, to obtain more navigation information for vehicluar positioning, the concept of hybrid positioning has been proposed [4]–[6]. The receiver uses radio frequency signals from signals of opportunity (SOOP), such as GSM/UMTS base stations, Wi-Fi and digital television DVB signals, to use as navigation measurements. However, such a hybrid navigation system relies on the direct line of sight measurements between the receiver on the vehicles and the SOOP signal sources. The hybrid system becomes unavailable when the vehicle is out of signal range. To reduce this deficiency, cooperative methods have been proposed in [7], [8] to overcome the lack of navigation measurement, which can provide reliable and better navigation performance with some inter-node measurements such as ultrawideband (UWB) communication and Bluetooth.

Some researchers have focused on non-Bayesian cooperative positioning (CP) [9]–[11], transforming the CP problem to a least squares (LS) problem, using Gauss-Newton or steepest descent to iteratively calculate the optimal results. However, the CP problems involve many variables and are not always a convex problem, so it is difficult to find the optimal results for a multivariable nonlinear problem. So, relaxing the non-Bayesian CP problem to a semi-definite programming problem (SDP) [12] or a cone programming problem [13] becomes a more robust solution.

The main shortcoming of non-Bayesian CP methods is the error accumulation caused by deterministic estimation of states, which can lead to severe performance degradation [14]. The Bayesian CP method can solve such problems, as it treats the navigation states as random variables. Based on the Bayesian deduction of navigation states, several belief propagation (BP) methods have been proposed to improve the navigation performance of single nodes in a network [15]–[17]. The research

in [18] presented a sum-product algorithm for wireless network (SPAWN) based on a net-factor graph and net-message passing schedule. The BP was applied to estimate the posterior marginal probability density function (PDF) of the agent's position. Simulation results showed that the cooperative scheme largely improves the absolute positioning ability of every single node. To make full use of GNSS data, research in [8] proposed a hybrid SPAWN (H-SPAWN) method which combines the ranging information from neighbour nodes and the pseudoranges obtained from GPS/GNSS "anchor nodes". This extends the application of SPAWN to more complex scenarios. Although the BP methods obviously have excellent positioning performance, their iterative computation of marginal PDF requires the integrals, which is typically computed using Monte Carlo integration with importance sampling. Therefore, they need large numbers of weighted samples (particles) to describe cooperative messages [19]. Such a heavy computation load restricts the practical application of the CP algorithm due to their weak real-time performance. To decrease the high computation complexity of classical CP, the universal cooperative localizer (UCL) [20] was proposed to simplify the message passing procedure to a generalized linear mixing problem. However, its application scenario is restricted to two-dimensional (2D) positioning, and when expanded into 3D to include the height dimension as required by many vehicular navigation applications (e.g. to detect if the vehicle is entering a ramp), it becomes computationally untenable.

Although the Bayesian CP methods mentioned above have good positioning performance, many of them are applied in a static scenario, or just describe the movement of nodes via simple motion models such as a constant velocity model [21] or a delta function without move direction [18]. Therefore, such CP methods will have performance degradation in a complex dynamic application environment. To overcome this problem, one effective approach is to combine CP method with Dead Reckoning (such as INS) to further improve the estimation accuracy. However, it is hard to directly insert Dead Reckoning computation into the CP structure. Also, combining traditional CP method with Dead Reckoning via a secondary estimator is a more practical approach.

Therefore, in this paper we propose a new hybrid-CP method based on generalized approximate message passing (GAMP) and Kalman filter for vehicular network applications, which can make full use of navigation measurements from an onboard INS, GNSS receiver, SOOP sources, ground stations and inter-node measurements of neighbour vehicles. Our method adopts the framework of GAMP [22] which exploits the central limit theorem and Taylor expansion to simplify the classical sampling mechanism in BP to a numerical computation process. For initialisation, we used a Kalman filter to provide the initial states and parameters to the GAMP.

The main contribution of this paper is to extend the GAMP to a hybrid cooperative positioning scenario in three dimensions (3D), and combine the GAMP with INS through a Kalman filter, which can provide cooperative navigation solutions for vehicles more precisely and efficiently. Results show that it has better positioning performance than multiple traditional CP methods.
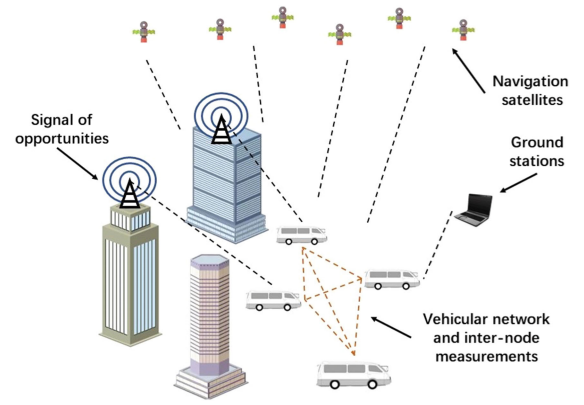

Fig. 1. Vehicular cooperative positioning in urban scenario.

They also show that the positioning performance of hybrid-CP in hybrid positioning scenarios improves with growing numbers of useful navigation measurements and cooperative neighbor nodes.

II. OBSERVATION MODEL

Consider a group of vehicles that carry out a mission (see Fig. 1) in an urban area, where the number of available satellites is not adequate for all vehicles. All vehicles share navigation and sensor data through a wireless network, and they are capable of receiving the signals from SOOP sources, such as digital television signals and GMS/UMTS signals. The mathematical model is composed of a set of vehicles and ground control stations of cardinality $\mathbb{N}$, a set of satellites $\mathbb{S}$ and a set of SOOP signal sources $\mathbb{O}$. Position variables of vehicle i are denoted by $\mathbf{x}_i = [x_i \ y_i \ z_i]$, velocity variables are denoted by $\mathbf{v}_i = [v_{i,x} \ v_{i,y} \ v_{i,z}]$, the location and velocity for N vehicles in a group are denoted by a concatenated vector $\mathbf{q} = [\cdots \ \mathbf{x}_i \ \cdots \cdots \ \mathbf{v}_i \ \cdots]$.

Here it should be notice that the concatenated vector $\mathbf{q}$ is also written as $\mathbf{q} = [\cdots, q_i, \cdots]$ in the follow parts, where q_i means the i-th element of state vector $\mathbf{q}$.

In the considered scenario, five types of measurements are used:

A. Double Differenced GNSS Pseudoranges

The GNSS pseudorange between satellite and vehicle is explained as:

$$\tilde{\rho}_{\alpha_n \leftrightarrow i} = R_{\alpha_n \leftrightarrow i} + c\delta_{\alpha_n} + c\delta_i + \zeta_{\alpha_n \leftrightarrow i} + b_{\tilde{\rho}} + \varepsilon_{\alpha_n \leftrightarrow i} \quad (1)$$

where $\alpha_n \in \mathbb{S}$, $i \in \mathbb{N}$, c is the speed of light, $R_{\alpha_n \leftrightarrow i}$ is the distance between vehicle i and satellite α_n, δ_{α_n} is the clock error of satellite α_n, δ_i is the clock error of onboard receiver of vehicle i, $\zeta_{\alpha_n \leftrightarrow i}$ is the error due to ionosphere, troposphere, and orbit of satellite α_n, $b_{\tilde{\rho}}$ is the error caused by multipath or non-line-of-sight (NLOS), and $\varepsilon_{\alpha_n \leftrightarrow i}$ is the error caused by receiver thermal noise. In (1), $\zeta_{\alpha_n \leftrightarrow i}$ and δ_{α_n} are the same for all vehicles within the communication range and can be eliminated by differencing the observation of any pair of onboard receivers, i.e., i and j, which observe a same satellite. In [23], the

double differencing can eliminate the errors caused by receivers' clock errors and correlated errors of GNSS observations by two receivers and two satellites. Then, it is well-known that the double differenced GNSS pseudorange observations can be defined as:

$$\Delta\nabla\tilde{\rho}_{\alpha_n\alpha_m\leftrightarrow i,j} = (\mathbf{e}^{\alpha_n} - \mathbf{e}^{\alpha_m})(\mathbf{x}_j - \mathbf{x}_i)^T + b_{\Delta\nabla\tilde{\rho}} + \varepsilon_\rho \quad (2)$$

where $\alpha_n, \alpha_m \in \mathbb{S}$, $i, j \in \mathbb{N}$, $\mathbf{e}^{\alpha_n}$ and $\mathbf{e}^{\alpha_m}$ are the unit vectors from vehicle i to the satellite α_n and α_m respectively. $\mathbf{x}_i$ is the location of vehicle i in an Earth Centred Earth Fixed (ECEF) frame, $b_{\Delta\nabla\tilde{\rho}}$ is the error for multipath or NLOS that cannot be removed by double differencing, the error ε_ρ for double differenced GNSS measurements can be denoted by an additive white Gaussian noise (AWGN) which is caused by the receiver thermal noise.

According to (2), the double differenced GNSS pseudorange Doppler shifts for vehicles i, j and satellites α_n, α_m can be obtained as:

$$\Delta\nabla\tilde{\vartheta}_{\alpha_n\alpha_m\leftrightarrow i,j} = \frac{1}{\lambda_G}(\mathbf{e}^{\alpha_n} - \mathbf{e}^{\alpha_m})^T(\mathbf{v}_j - \mathbf{v}_i) + \varepsilon_\vartheta \quad (3)$$

where λ_G is the wavelength of GNSS signal, $\mathbf{v}_j$ is the velocity of vehicle i in an ECEF frame, ε_ϑ is AWGN for measurements.

B. UWB Ranges

UWB transceivers are widely used as a communication and ranging sensor in both indoor and outdoor environments [24], [25]. There were many researches that using UWB as the vehicle-to-vehicle (V2V) and vehicle-to-infrastructure (V2I) ranging sensor [26], [27], [28]. In this paper, UWB ranging is used as the V2V and V2I (ground station) measurements. The UWB ranging between node i and j is:

$$\tilde{r}_{i\leftrightarrow j} = \|\mathbf{x}_i - \mathbf{x}_j\| + b_{\tilde{r}} + \varepsilon_r \quad (4)$$

where the symbol $\|\ \|$ denotes the Euclidean distance, $b_{\tilde{r}}$ is the bias caused by NLOS, ε_r is AWGN for inter-node range measurements.

C. TDOA Measurements From SOOP Sources

Although the GNSS receiver can provide reliable navigation measurements in most cases, GNSS signals are often blocked by the urban buildings or any other certain terrain. Several novel positioning methods based on signals of opportunity were proposed to solve this problem [29], [30]. In this work, the SOOP measurements based on time-difference of arrival (TDOA) were used to provide more navigation information. TDOA based SOOP signal are widely used in opportunistic positioning because they do not require clock synchronization. The SOOP signal from vehicle j to vehicle i via the SOOP source g can be denoted as:

$$\tilde{d}_{j\rightarrow i} = (\|\mathbf{x}_g - \mathbf{x}_j\| - \|\mathbf{x}_g - \mathbf{x}_i\|) + b_{\tilde{d}} + \varepsilon_d \quad (5)$$

where $g \in \mathbb{O}$, $\mathbf{x}_g$ is the location of SOOP signal source in an ECEF frame, $b_{\tilde{d}}$ is the NLOS or multipath bias, ε_d are zero mean Gaussian to model errors for TDOA measurements.

D. Closed-Loop Doppler Measurements

In the area of ITS positioning techniques, dedicated short-range communications (DSRC) are considered as a promising supplement navigation sensor. Many methods were proposed recently using DSRC Doppler as the additional measurements to augment the existing navigation system [31], [32]. The DSRC Doppler is essentially the Closed-loop Doppler [33], the measurements between node i and j is defined as:

$$\tilde{d}p_{i\leftrightarrow j} = \frac{(\mathbf{v}_i - \mathbf{v}_j) \cdot \mathbf{e}_{i\rightarrow j}}{\lambda_R} + \varepsilon_f \quad (6)$$

where $\mathbf{e}_{i\rightarrow j}$ is the unit vector between vehicle i and vehicle j, λ_R is the wavelength of the ranging signal in meters, ε_f is AWGN for Doppler measurements.

III. HYBRID COOPERATIVE POSITIONING

Fig. 2 shows the architecture of the proposed hybrid cooperative positioning method. It is essentially a tight integration between the GAMP algorithm and Kalman filter. In this architecture, GAMP is a centralized way to process the measurements of all vehicles, and the Kalman filter is a decentralized processing for each vehicle.

GAMP is used to fuse all the possible navigation measurements. It will output the position estimation and the corresponding variance information after convergence, these data will be used in the initialization of covariance matrix for the Kalman filter. The Kalman filter can fuse the information from GAMP and INS to get a further estimation. The posterior covariance matrix of Kalman filter and the modified INS data will then be used in the initialization of GAMP at the next epoch.

In most Kalman filter based CP methods, their time updates of the navigation states and covariance matrix are based on the Kalman filter itself. But for the proposed method, its covariance matrix and navigation states are updated based on the GAMP estimation. And for the common GAMP application such as the UCL in [20], it is more like a "snapshot" algorithm without temporal cooperation. In the proposed method, the navigation states and variance estimation of GAMP is doing a further temporal cooperation based on the INS and Kalman filter.

A. Problem Model

It is reasonable to assume that the location and velocity of all vehicles at epoch t are independent, so the prior distribution of navigation states for all vehicles can be denoted as:

$$p\left(\frac{\mathbf{q}^{(t)}}{\boldsymbol{\mu}^{(t)}}\right) = \prod_i p\left(\frac{q_i^{(t)}}{\mu_i^{(t)}}\right) \quad (7)$$

where $\boldsymbol{\mu}^{(t)}$ is the vector of a *priori* navigation states (i.e. position and velocity). It can be initialised from the navigation results of GPS/INS integration system, $q_i^{(t)}$ is the i-th element of navigation state $\mathbf{q}^{(t)}$, $\mu_i^{(t)}$ is the i-th element of $\boldsymbol{\mu}^{(t)}$.

Also, each measurement for every vehicle at epoch t is independent, the *posterior* distribution of all measurements can be
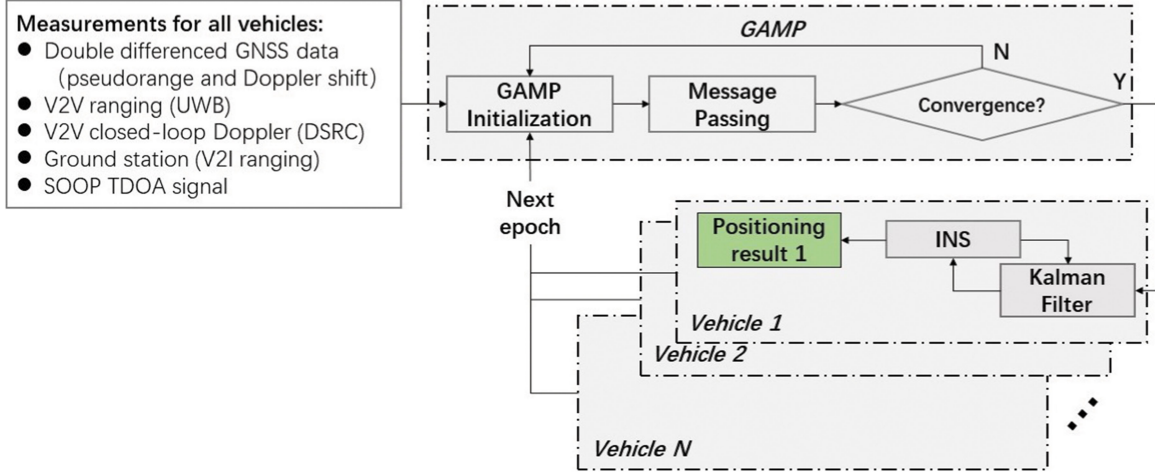
Fig. 2.   Structure of hybrid cooperative positioning.

described as:

$$p\left(\frac{\tilde{\mathbf{m}}^{(t)}}{\mathbf{f}^{(t)}}\right) = \prod_j p\left(\frac{\tilde{m}_j^{(t)}}{f_j^{(t)}}\right) \qquad (8)$$

where $\mathbf{f}^{(t)}$ is the set of all functions between navigation states and measurements, $\tilde{m}_j^{(t)}$ is the j-th measurement set of all measurements $\tilde{\mathbf{m}}^{(t)}$ at epoch t, $f_j^{(t)}$ is the j-th function of the set of functions at epoch t. In a normal case, the measurement errors used in the proposed method are assumed always to be normal distributed. For the faulty cases caused by non-line-of-sight (NLOS) or multipath, such faulty measurements can be removed by some integrity methods [34], [35]. Although the problem of faulty measurements is not within the scope of this paper, we still take the NLOS and multipath into consideration in the simulation (Section IV).

Based on the definition above, the goal of hybrid cooperative localizer is to find the *posterior* distribution of $\mathbf{q}^{(t)}$ at epoch t based on all measurements $\tilde{\mathbf{m}}^{(t)}$. In this work, the movement of every vehicle is modelled as a Markov process [36]. Then, the posterior distribution of all navigation states $\mathbf{q}^{(t)}$ at epoch t can be simplified as:

$$p\left(\frac{\mathbf{q}^{(t)}}{\boldsymbol{\mu}^{(t)}, \tilde{\mathbf{m}}^{(t)}}\right) = p\left(\frac{\tilde{\mathbf{m}}^{(t)}}{\mathbf{q}^{(t)}}\right) p\left(\frac{\mathbf{q}^{(t)}}{\boldsymbol{\mu}^{(t)}}\right) \Big/ p\left(\frac{\mathbf{m}^{(t)}}{\boldsymbol{\mu}^{(t)}}\right)$$

$$\propto p\left(\frac{\tilde{\mathbf{m}}^{(t)}}{\mathbf{q}^{(t)}}\right) p\left(\frac{\mathbf{q}^{(t)}}{\boldsymbol{\mu}^{(t)}}\right)$$

$$= \prod p\left(\frac{\tilde{m}_n^{(t)}}{f_n^{(t)}}\right) \prod p\left(\frac{q_i^{(t)}}{\mu_i^{(t)}}\right) \qquad (9)$$

Then the relationship between the navigation states $\mathbf{q}^{(t)}$ and the measurements $\tilde{\mathbf{m}}^{(t)}$ can be described by a factor graph as in Fig. 3. It consists of factor nodes and variable nodes, which represent the relationship between measurement and navigation state respectively.
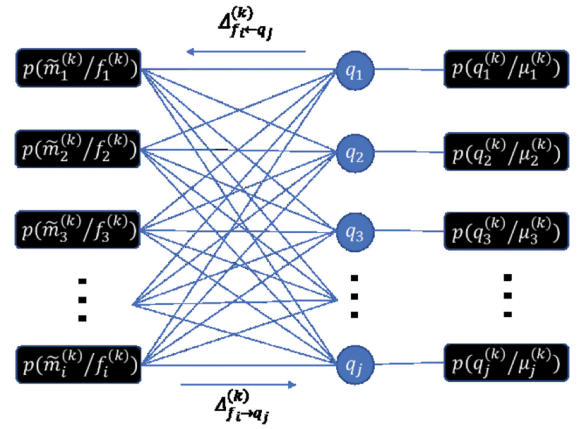

Fig. 3.   Factor graph for navigation states.

B. Generalized Approximate Message Passing

To simplify the notation, the superscript (t) is omitted in this section, and the superscript (k) denotes k-th iteration of GAMP computation at epoch t.

Fig. 3 shows the GAMP model definition. $\Delta_{f_i \leftarrow q_j}^{(k)}$ is the message from variable node to factor node, and indicates the cooperative contribution from the variable distribution of $q_j^{(k)}$ during cooperative estimation. $\Delta_{f_i \rightarrow q_j}^{(k)}$ is the message from factor node to variable node, and represents the cooperative modification information from measurements to the variable.

In the context of GAMP, the messages $\Delta_{f_i \leftarrow q_j}^{(k)}, \Delta_{f_i \rightarrow q_j}^{(k)}, \Delta_{q_j}^{(k)}$ always refer to the log probability distribution of the measurement function f_i in case of navigation state estimation $q_j^{(k)}$, the navigation state $q_j^{(k)}$ in case of measurement function f_i and navigation state q_j at k-th GAMP iteration, respectively.

The message $\Delta_{f_i \leftarrow q_j}^{(k)}$ and $\Delta_{f_i \rightarrow q_j}^{(k)}$ can be defined as [22]:

$$\Delta_{f_i \leftarrow q_j}^{(k)} = c_\Delta + \log p\left(\frac{q_j^{(k)}}{\mu_j^{(k)}}\right) + \sum_{f_l \neq f_i} \Delta_{f_l \rightarrow q_j}^{(k)} \qquad (10)$$

$$\Delta_{f_i \to q_j}^{(k)} = c_\Delta + \log \int p\left(\frac{\tilde{m}_i^{(k)}}{f_i^{(k)}}\right) \prod_{r \neq j} \exp \Delta_{f_i \leftarrow q_r}^{(k)} \quad (11)$$

where c_Δ is the constant value.

Based on the GAMP model definition, if the marginal posterior distribution of the j-th vehicle's navigation state q_j achieves convergence after n GAMP iterations, it can be calculated from (10) by incorporating (11):

$$\Delta_{q_j} = c_\Delta + \log p\left(\frac{q_j^{(n)}}{\mu_j^{(n)}}\right) + \sum_{f_i \in M_j} \Delta_{f_l \to q_j}^{(n)} \quad (12)$$

where M_j is the set of measurements related to vehicle j. The terminal condition of convergence is discussed in *section D*.

The set of all available measurements for all vehicles is defined as:

$$\tilde{\mathbf{m}} = \begin{bmatrix} \tilde{r} & \Delta\nabla\tilde{\rho} & \Delta\nabla\tilde{\vartheta} & \tilde{dp} & \tilde{d} \end{bmatrix}^T \quad (13)$$

where, $\tilde{r} = [\ldots \tilde{r}_{i \leftrightarrow j} \cdots]^T$ is the vector of inter-node range measurements, $\Delta\nabla\tilde{\rho} = [\ldots \Delta\nabla\tilde{\rho}_{s_n s_m \leftrightarrow i,j} \cdots]^T$ is the vector of double differenced GNSS pseudoranges, $\Delta\nabla\tilde{\vartheta} = [\ldots \Delta\nabla\tilde{\vartheta}_{s_n s_m \leftrightarrow i,j} \cdots]^T$ is the vector of double differenced GNSS pseudorange Doppler, $\tilde{dp} = [\ldots \tilde{dp}_{i \leftrightarrow j} \cdots]^T$ is the vector of Doppler measurements from neighbour nodes, $\tilde{d} = [\cdots \tilde{d}_{j \to i} \cdots]^T$ is the vector of TDOA measurements from SOOP signal sources.

To simplify the description of cooperative messages via CLT, GAMP applies linearization to model relationships between measurements and states [22]. By taking the Taylor expansion, the measurement $\tilde{\mathbf{m}}$ can be linearly approximated by the following, given estimated navigation state $\hat{\mathbf{q}}^{(k)}$:

$$\tilde{\mathbf{m}}^{(k)} = \hat{\mathbf{m}}^{(k)} + \mathbf{A}^{(k)}\left[\mathbf{q}^{(k)} - \hat{\mathbf{q}}^{(k)}\right] + \mathbf{n} \quad (14)$$

where $\hat{\mathbf{m}}^{(k)}$ is the expected (*apriori*) measurements given estimated navigation state $\hat{\mathbf{q}}^{(k)}$, $\mathbf{n}$ is the AWGN noise vector, $\mathbf{A}^{(k)}$ is Jacobian matrix:

$$\mathbf{A}^{(k)} = \left.\frac{\partial \mathbf{m}}{\partial \mathbf{q}}\right|_{\mathbf{q} = \hat{\mathbf{q}}^{(k)}} \quad (15)$$

Then the measurement vector of all vehicles $\tilde{\mathbf{m}}$ in (15) can be rewritten as:

$$\tilde{\mathbf{m}} = \mathbf{f}\left(\mathbf{q}^{(k)}\right) + \mathbf{n} \quad (16)$$

where $\mathbf{f}(\mathbf{q}^{(k)}) = \mathbf{A}^{(k)}\mathbf{q}^{(k)} + [\hat{\mathbf{m}}^{(k)} - \mathbf{A}^{(k)}\hat{\mathbf{q}}^{(k)}]$.

Therefore, the message $\Delta_{f_i \to q_j}^{(k)}$ emitted by factor nodes in (11) is approximated by:

$$\Delta_{f_i \to q_j}^{(k)} \approx c_\Delta + \log \int p\left(\frac{\tilde{m}_i}{[\mathbf{f}(\mathbf{q}^{(k)})]_i}\right) \prod_{r \neq j} \exp \Delta_{f_i \leftarrow q_r}^{(k)} \quad (17)$$

where $\tilde{m}_i$ is the i-th element of measurement $\tilde{\mathbf{m}}$, $[\cdot]_i$ denotes the i-th element of vector. Here, we define $\mathbf{G}^{(k)}$ as the *posteriori* residual vector computed as:

$$\mathbf{G}^{(k)} = \hat{\mathbf{m}}^{(k)} - \mathbf{A}^{(k)}\hat{\mathbf{q}}^{(k)} \quad (18)$$

So, according to CLT, the message $\Delta_{f_i \to q_j}^{(k)}$ emitted by a factor node can be further derived as:

$$\Delta_{f_i \to q_j}^{(k)} \approx c_\Delta + H\left(\hat{p}_i^{(k)}, \tilde{m}_i, \tau_{i,p}^{(k)}\right) \quad (19)$$

where function $H(\cdot)$ is the simplified representation, $\hat{p}_i^{(k)}$ and $\tau_{i,p}^{(k)}$ are the estimated mean and variance of i-th measurement function f_i respectively (see (61), (62)). Taking the second order Taylor-expansion of message $\Delta_{f_i \to q_j}^{(k)}$, we can rewrite (20) as:

$$\Delta_{f_i \to q_j}^{(k)} \approx c_\Delta + \left(\hat{s}_i^{(k)} a_{i,j}^{(k)} + \tau_{i,s}^{(k)} a_{i,j}^{(k)2} q_{f_i \leftarrow q_j}^{(k)}\right) q_j^{(k)}$$
$$- \frac{\tau_{i,s}^{(k)}}{2} a_{i,j}^{(k)2} q_j^{(k)2} \quad (20)$$

where, $q_{f_i \leftarrow q_j}^{(k)}$ is the estimate of j-th navigation state $q_j^{(k)}$ at k-th iteration, $\hat{s}_i^{(k)}$ and $\tau_{i,s}^{(k)}$ are the first and second order terms of message $\Delta_{f_i \to q_j}^{(k)}$ (see (64), (65)). Substituting the message emitted by factor node in (21) into the message from variable node to factor node $\Delta_{f_i \to q_j}^{(k)}$ in (11), the message emitted by variable node $q_j^{(k)}$ is rewritten as:

$$\Delta_{f_i \leftarrow q_j}^{(k)} \approx c_\Delta + \log\left[p\left(\frac{q_j^{(k)}}{\mu_j^{(k)}}\right) N\left(q_j^{(k)}; \hat{r}_{f_i \leftarrow q_j}^{(k)}, \tau_{r,j}^{(k)}\right)\right] \quad (21)$$

where, $N(a; b, c)$ is the Gaussian function of variable a with b and c as its mean and variance respectively, $\hat{r}_{f_i \leftarrow q_j}^{(k)}$ and $\tau_{r,j}^{(k)}$ are the estimated mean and variance of all incoming messages from factor nodes to variable node $q_j^{(k)}$ (see (67), (68)) respectively. The detailed derivations of (19)∼(21) are summarized in the appendix.

According to (21), the message of the j-th navigation state in (12) can be simplified as:

$$\Delta_{q_j}^{(k)} = c_\Delta + \log\left[p\left(\frac{q_j^{(k)}}{\mu_j^{(k)}}\right) N\left(q_j^{(k)}; \hat{r}_j^{(k)}, \tau_{r,j}^{(k)}\right)\right] \quad (22)$$

Finally, the marginal distribution of the j-th navigation state in k-th iteration $q_j^{(k)}$ is:

$$p\left(\frac{q_j^{(k)}}{\mu_j^{(k)}, \hat{r}_{q_j}^{(k)}; \tau_{r,j}^{(k)}}\right) \propto p\left(\frac{q_j^{(k)}}{\mu_j^{(k)}}\right) N\left(q_j^{(k)}; \hat{r}_j^{(k)}, \tau_{r,j}^{(k)}\right) \quad (23)$$

Taking the mean of this distribution yields the minimum mean squared error (MMSE) estimate of navigation state $q_j^{(k)}$. A termination judgment is needed to decide whether the calculation of $q_j^{(k)}$ was converged to a proper value.

In summary, under the framework of GAMP, the message passing procedure in traditional BP becomes a scalar computation procedure. The first part is to initialize the navigation state $\mathbf{q}^{(0)}$ and calculate the Jacobian matrix $\mathbf{A}^{(k)}$ in (15) and $\mathbf{G}^{(k)}$ in (18) according to the observation model in (2)∼(6). The second part is to compute the mean $\hat{p}_i^{(k)}$ and variance $\tau_{i,p}^{(k)}$ of i-th measurement function f_i in (19); first order term $\hat{s}_i^{(k)}$ and second order term $\tau_{i,s}^{(k)}$ of message $\Delta_{f_i \to q_j}^{(k)}$ in (20); mean $\tau_{r,j}^{(k)}$

and variance $\hat{r}_j^{(k)}$ in (22); and the j-th navigation state estimation in k-th iteration $q_j^{(k)}$ of (23). The final part is the termination judgment: the algorithm will re-iterate until navigation state $q_j^{(k)}$ is within a tolerance. After all the $q_j^{(k)}$ converges to the certain value, GAMP will output the *priori* position estimation of all the states:

$$\mathbf{q}^{(t/t-1)} = \left[\cdots , q_j^{(k)}, \cdots \right] \tag{24}$$

The step-by-step procedure of GAMP based hybrid-CP is introduced in section *D*.

C. INS/GAMP Integration

Filters are per se estimation engines to refine the estimation through mobility models, which can give a second estimation of navigation state [21]. To make full use of onboard INS of vehicles, an INS/GAMP integration method is used to enhance the performance of GAMP.

Noticing that the GAMP used in this work belongs to a long line of methods based on Gaussian and quadratic approximation of belief propagation (BP), which is the simplification of sum-product BP for computations of MMSE estimates. According to the analysis and results in references [22], [37], [38], if the noise in the input function for GAMP follows a zero-mean Gaussian distribution, the estimated results will also follow the Gaussian distribution, their mean will converge to the true value after certain iteration, and the estimation will asymptotically approach the Cramer-Rao lower bound. Therefore, for the application of GAMP in CP, if the measurement noises for vehicles are obeying the zero-mean Gaussian distribution in normal case, the estimated navigation states of GAMP will also following Gaussian distributions with the mean of the true value, which is the foundation of INS/GAMP integration.

The INS error equation is used as the system state equation:

$$\mathbf{X} = [\phi_e, \phi_n, \phi_u, \delta v_e, \delta v_n, \delta v_u, \delta L, \delta\lambda, \delta h,$$

$$\varepsilon_{b,x}, \varepsilon_{b,y}, \varepsilon_{b,z}, \varepsilon_{r,x}, \varepsilon_{r,y}, \varepsilon_{r,z}, \nabla_x, \nabla_y, \nabla_z] \tag{25}$$

where, ϕ_e, ϕ_n, ϕ_u are the misalignment angle errors; $\delta v_e, \delta v_n, \delta v_u$ are the velocity in an east, north, and up (ENU) coordinates; $\delta L, \delta\lambda, \delta h$ are the latitude, longitude and height respectively; $\varepsilon_{b,x}, \varepsilon_{b,y}, \varepsilon_{b,z}, \varepsilon_{r,x}, \varepsilon_{r,y}, \varepsilon_{r,z}$ are the gyro constant drift errors and the first-order Markov drift errors respectively; $\nabla_x, \nabla_y, \nabla_z$ are the accelerometer biases.

The state error equation of the INS is:

$$\dot{\mathbf{X}} = \mathbf{F}\mathbf{X} + \mathbf{B}\mathbf{W} \tag{26}$$

where $\mathbf{F}$ is the linearized INS error states matrix, $\mathbf{B}$ is the noise transfer matrix, $\mathbf{W}$ is the system process noise which is determined by the parameters of the accelerometer and gyro, and has zero mean multivariate normal distribution with variance $\mathbf{Q}$.

The observation model of integration is:

$$\mathbf{Y}_G = \mathbf{H}_G \mathbf{X} + \mathbf{V}_G \tag{27}$$

where, $\mathbf{Y}_G$ is the observation vector related to GAMP estimation, $\mathbf{H}_G$ is the observation matrix, $\mathbf{V}_G$ is the measurement noise of GAMP with variance matrix $\mathbf{R}_G$.

The observation vector, observation matrix and noise and variance matrix are defined as:

$$\mathbf{Y}_G = \begin{bmatrix} \mathbf{x} - \mathbf{x}_{ins} \\ \mathbf{v} - \mathbf{v}_{ins} \end{bmatrix} \tag{28}$$

$$\mathbf{H}_G = \begin{bmatrix} 0_3 & 0_3 & \text{diag}\left[R_M, R_N \cos L, 1\right] & 0_{3\times9} \\ 0_3 & I_3 & 0_3 & 0_{3\times9} \end{bmatrix} \tag{29}$$

$$\mathbf{R}_G = \text{diag}\left[\boldsymbol{\tau}_\mathbf{x}, \boldsymbol{\tau}_\mathbf{v}\right] \tag{30}$$

where, $\mathbf{x}$ and $\mathbf{v}$ are the position and velocity estimates, which come from the GAMP estimated concatenated vector $\mathbf{q}^{(t/t-1)}$ in (24), R_M and R_N are the curvature radii of the reference ellipsoid in longitude and latitude circles of the earth, $\boldsymbol{\tau}_\mathbf{x}$ and $\boldsymbol{\tau}_\mathbf{v}$ are their corresponding variance in (50).

Having $\mathbf{F}$, $\mathbf{B}$, $\mathbf{H}_G$, $\mathbf{Q}$ and $\mathbf{R}_G$, the standard equations of the Kalman filter for the proposed hybrid-CP method can now be implemented via [39].

In the Kalman filter, the *posteriori* estimate variance matrix $\mathbf{P}^+$ can be used to evaluate the estimation accuracy, which is updated using the following equation:

$$\mathbf{P}(t)^+ = \left[\mathbf{I} - \mathbf{K}(t)\mathbf{H}_G(t)\right]\mathbf{P}(t)^- \left[\mathbf{I} - \mathbf{K}(t)\mathbf{H}_G(t)\right]^T$$
$$+ \mathbf{K}(t)\mathbf{R}_G(t)\mathbf{K}(t)^T \tag{31}$$

where, $\mathbf{P}^-$ is the *priori* variance matrix, $\mathbf{K}$ is the filter gain and $\mathbf{I}$ is the corresponding identity matrix. The *priori* variance matrix $\mathbf{P}^-$ and filter gain $\mathbf{K}$ are calculated by:

$$\mathbf{P}(t)^- = \mathbf{F}(t)\mathbf{P}(t-1)^+\mathbf{F}(t)^T + \mathbf{B}\mathbf{Q}\mathbf{B}^T \tag{32}$$

$$\mathbf{K}(t) = \mathbf{P}(t)^-\mathbf{H}_G(t)$$
$$\left[\mathbf{H}_G(t)\mathbf{P}(t)^-\mathbf{H}_G(t)^T + \mathbf{R}_G(t)\right]^{-1} \tag{33}$$

The variance of the estimated state vector can be predicted by (33), which is largely depend on the GAMP generated variance matrix $\mathbf{R}_G$ and the INS determined variance matrix $\mathbf{Q}$.

In each Kalman filter iteration, each vehicle i can compute its filtered position $\mathbf{x}_{i,ins}$ and velocity $\mathbf{v}_{i,ins}$ from onboard INS, and update their variance $\boldsymbol{\tau}_{i,\mathbf{x}}$ and $\boldsymbol{\tau}_{i,\mathbf{v}}$ by the corresponding diagonal elements in the *posteriori* variance matrix $\mathbf{P}^+$. Thus the outputs of the Kalman filter are the posterior states estimation $\mathbf{q}^{(t/t)}$ and the corresponding posterior variance $\boldsymbol{\tau}^{(t/t)}$:

$$\mathbf{q}^{(t/t)} = \left[\cdots \mathbf{x}_{i,ins}(t) \cdots \cdots \mathbf{v}_{i,ins}(t) \cdots \right] \tag{34}$$

$$\boldsymbol{\tau}^{(t/t)} = \left[\cdots \boldsymbol{\tau}_{i,\mathbf{x}}(t) \cdots \cdots \boldsymbol{\tau}_{i,\mathbf{v}}(t) \cdots \right] \tag{35}$$

Then the initial value of states and *priori* variance for GAMP in the next epoch can be set according to the $\mathbf{q}^{(t/t)}$ and $\boldsymbol{\tau}^{(t/t)}$.

D. Algorithm Description

Fig. 4 shows the procedure for the hybrid-CP algorithm. Where the GAMP is used to fuse the multi-sensor measurements, then Kalman filter can update the variance of the navigation state, and INS is used to provide the navigation results.

1) Initialization: The first step is to initialize the parameters for GAMP calculation. After the navigation algorithm starts, if it is the first epoch of navigation, the initial navigation
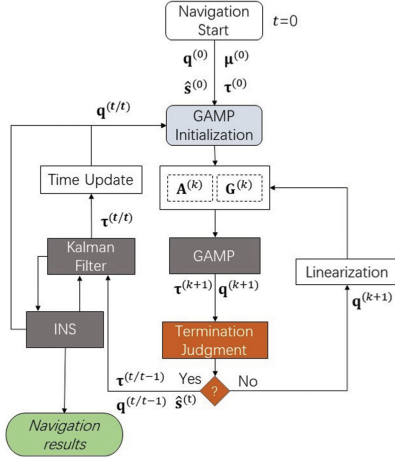
Fig. 4.　Procedure for hybrid-CP.

states $\mathbf{q}^{(0)}$ can be provided by a GPS/INS solution or initial alignment of INS; otherwise it can be updated by the filtered navigation state $\boldsymbol{\mu}^{(0)} = \mathbf{q}^{(t/t)}$ and its corresponding variance $\boldsymbol{\tau}^{(0)} = \boldsymbol{\tau}^{(t/t)}$. $\boldsymbol{\mu}^{(0)} = [\ldots \ \mu_j^{(0)} \ \ldots]$ and $\boldsymbol{\tau}^{(0)} = [\ldots \ \tau_j^{(0)} \ \ldots]$ are the *priori* mean and variance of $\mathbf{q}^{(0)}$ respectively; the matrix $\mathbf{A}^{(0)}$ is calculated based on $\mathbf{q}^{(0)}$; the concatenated vector $\hat{\mathbf{s}}^{(0)} = [\ldots \ \hat{s}_i^{(0)} \ \ldots]$, where each element is set to 0, threshold α is set to a small positive value, and the break condition is $\|\mathbf{q}^{(k+1)} - \mathbf{q}^{(k)}\|/\|\mathbf{q}^{(k+1)}\| < \alpha$.

2) *Calculation of mean $\hat{p}_i^{(k)}$ and variance $\tau_{i,p}^{(k)}$ of measurement function f_i in (19):*

$$\tau_{i,p}^{(k)} = \sum_l a_{i,l}^{(k)2} \tau_l^{(k)} \qquad (36)$$

$$\hat{p}_i^{(k)} = \sum_l a_{i,l}^{(k)} q_{f_i \leftarrow q_j}^{(k)} + [\mathbf{G}^{(k)}]_i \qquad (37)$$

According to the approximation deduced in [36], (37) can be rewritten recursively as:

$$\hat{p}_i^{(k)} = \sum_l a_{i,l}^{(k)} \hat{q}_j^{(k)} - \tau_{i,p}^{(k)} \hat{s}_i^{(k-1)} + [\mathbf{G}^{(k)}]_i \qquad (38)$$

3) *Calculation of mean $\hat{s}_i^{(k)}$ and variance $\tau_{i,s}^{(k)}$ of message $\Delta_{f_i \to q_j}^{(k)}$ in (20):*

$$\hat{s}_i^{(k)} = \frac{1}{\tau_{i,p}^{(k)}} \left[E\left(f_i^{(k)} | \hat{p}_i^{(k)}, \tilde{m}_i, \tau_{i,p}^{(k)} \right) - \hat{p}_i^{(k)} \right] \qquad (39)$$

$$\tau_{i,s}^{(k)} = \frac{1}{\tau_{i,p}^{(k)}} \left[1 - \frac{\text{var}\left(f_i^{(k)} | \hat{p}_i^{(k)}, \tilde{m}_i, \tau_{i,p}^{(k)} \right)}{\tau_{i,p}^{(k)}} \right] \qquad (40)$$

where the expectation $E(f_i^{(k)} | \hat{p}_i^{(k)}, \tilde{m}_i, \tau_{i,p}^{(k)})$ is proportional to $p(\frac{f_i^{(k)}}{\tilde{m}_i}) N(\tilde{f}_i^{(k)}; \hat{p}_i^{(k)}, \tau_{i,p}^{(k)})$, and for hybrid-CP applications, the distribution of relationships between navigation measurements and navigation states are $p(\frac{f_i^{(k)}}{\tilde{m}_i}) \sim N(f_i^{(k)}; \tilde{m}_i, \sigma_i^2)$. So, (39)

and (40) become:

$$\hat{s}_i^{(k)} = \frac{f_i^{(k)} - \hat{p}_i^{(k)}}{\tau_{i,p}^{(k)} + \sigma_i^2} \qquad (41)$$

$$\tau_{i,s}^{(k)} = \frac{1}{\tau_{i,p}^{(k)} + \sigma_i^2} \qquad (42)$$

4) *Calculation of mean $\hat{r}_{f_i \leftarrow q_j}^{(k)}$ and variance $\tau_{rij}^{(k)}$ of message from all other factor nodes to variable nodes $q_j^{(k)}$ (see(21)):*

$$\hat{r}_j^{(k)} = q_j^{(k)} + \tau_{r,j}^{(k)} \sum_{f_n} \hat{s}_n^{(k)} a_{n,j}^{(k)} \qquad (43)$$

$$\tau_{r,j}^{(k)} = \sum_{f_n} \left(\tau_{n,s}^{(k)} a_{n,j}^{(k)2} \right)^{-1} \qquad (44)$$

5) *Updating the GAMP navigation states estimation $q_j^{(k+1)}$ and its corresponding variance $\tau_j^{(k+1)}$ from:*

$$q_j^{(k+1)} = E\left[q_j^{(k)} | \mu_j^{(k)}, \hat{r}_j^{(k)}; \tau_{r,j}^{(k)} \right] \qquad (45)$$

$$\tau_j^{(k+1)} = \text{var}\left[q_j^{(k)} | \mu_j^{(k)}, \hat{r}_j^{(k)}; \tau_{r,j}^{(k)} \right] \qquad (46)$$

Because navigation state q_j (see (23)) is proportional to the distribution $p(\frac{q_j^{(k)}}{\mu_j^{(k)}}) N(q_j^{(k)}; \hat{r}_j^{(k)}, \tau_{r,j}^{(k)})$, and the distribution $p(\frac{q_j^{(k)}}{\mu_j^{(k)}})$ obeys the Gaussian distribution $N(q_j^{(k)}; \mu_j^{(k)}, \tau_j^{(k)})$, then (45) and (46) becomes:

$$q_j^{(k+1)} = \frac{\mu_j^{(k)} \tau_{r,j}^{(k)} + \hat{r}_j^{(k)} \tau_j^{(k)}}{\tau_j^{(k)} + \tau_{r,j}^{(k)}} \qquad (47)$$

$$\tau_j^{(k+1)} = \frac{\tau_{r,j}^{(k)} \tau_j^{(k)}}{\tau_j^{(k)} + \tau_{r,j}^{(k)}} \qquad (48)$$

6) *Threshold judgment:* If the threshold value satisfies the break condition in Step 1, the algorithm will stop and output the GAMP based navigation estimation $\mathbf{q}^{(t/t-1)}$, variance estimation $\boldsymbol{\tau}^{(t/t-1)}$ and vector $\hat{\mathbf{s}}^{(t)}$:

$$\mathbf{q}^{(t/t-1)} = \begin{bmatrix} \cdots & q_j^{(k+1)} & \cdots \end{bmatrix} \qquad (49)$$

$$\boldsymbol{\tau}^{(t/t-1)} = \begin{bmatrix} \cdots & \tau_j^{(k+1)} & \cdots \end{bmatrix} \qquad (50)$$

$$\hat{\mathbf{s}}^{(t)} = \begin{bmatrix} \cdots & \hat{s}_i^{(k)} & \cdots \end{bmatrix} \qquad (51)$$

Otherwise, it will update matrix $\mathbf{A}^{(k+1)}$ through (15) and updates the matrix $\mathbf{G}^{(k+1)}$ using (18), go back to step 2.

7) *Joint Estimation of GAMP and INS via Kalman Filter:* Using $\mathbf{q}^{(t/t-1)}$ and $\boldsymbol{\tau}^{(t/t-1)}$ as the input observation and the observation variance respectively, the estimation of GAMP can be integrated with the onboard INS. The new variance $\boldsymbol{\tau}^{(t/t)}$ from posteriori covariance matrix $\mathbf{P}^+$, and new navigation state estimation $\mathbf{q}^{(t/t)}$ from modified INS data can be used to initialize the GAMP iteration in next epoch. Output the navigation results $\mathbf{q}^{(t/t)}$, and go back to step 1 for the next epoch.
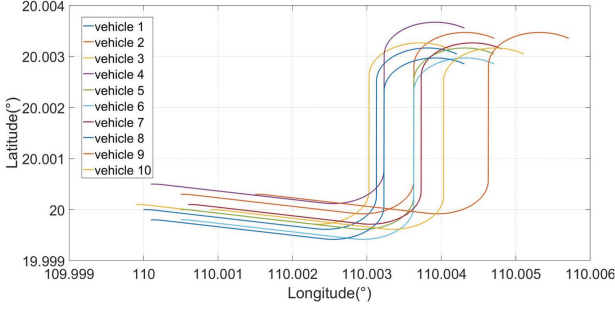
Fig. 5.   Trajectories for simulated vehicles.

E. Computation Complexity for GAMP

For the GAMP algorithm, the main computation load comes from the matrix multiplications in (36), (38), (43) and (44), so the computation burden for variable j is mainly based on the numbers of other variables that are related to it. In this way, the computation load for variable j is $O(I_G|M_j|)$ for I_G iteration, where M_j is the set of measurements related to vehicle j. For the message passing method using a sum-product algorithm over a factor graph like SPAWN, its complexity is dominated by message multiplication needed in messages from variable nodes to factor nodes and messages between different factors for every particle. So the SPAWN computation burden for variable j which requires I_B iterations and N particles is $O(I_B N|M_j|^2)$. Therefore, the hybrid-CP has lower computation complexity than that of SPAWN and conventional BP based CP algorithms.

IV. SIMULATION RESULTS

A. Simulation Configuration

Based on the background of urban scenario, a multi-vehicle system is simulated to verify the proposed hybrid-CP method. To fully assess the performance, all the results in this section are based on 200 Monte Carlo simulation trials.

Fig. 5 shows the trajectories for all vehicles during simulation, all the vehicles have an INS and GPS receiver as the fundamental positioning equipment, using the Ultra-wideband (UWB) and the Dedicated Short Range Communications (DSRC) as the measurement method between two vehicles, their working distances are set to 70 m [1] and 480 m [40] respectively. During the simulation, one ground station and two SOOP sources are simulated in view, and all the vehicles can communicate data with peers if their distance is lower than a certain value.

Based on the measurement models in (1)–(6), in nominal cases, the measurement noises are considered as AWGN. For GNSS, the random part of measurement error for carrier-smoothed-code pseudorange is lower than 2 m, according to reference [41]. We set the standard deviation of pseudorange and its Doppler shift to 1.4 m and 7 Hz (GPS L1 frequency) respectively. For UWB ranging, if signal is line-of-sight (LOS), the experimental results of our previous work shows the distribution of UWB error is a zero-mean Gaussian distribution with variance of 0.3 m^2 [1]. Referring to the closed-loop Doppler configuration of DSRC operating at 5.9 GHz, [31] shows the noise of DSRC

TABLE I
SENSOR CONFIGURATION AND SIMULATION PARAMETERS

Sensor	Parameter	Value
Gyro	Constant drift	10deg/h
	Gaussian noise standard dev.	10deg/h
	First-order Markov drift bias	10deg/h
	First-order Markov time	3600s
Accelerometer	First-order Markov bias	0.01g
	First-order Markov time	1800s
GNSS	Pseudorange noise standard dev.	1.4m
	Pseudorange doppler noise standard dev.	7Hz
UWB	Gaussian noise variation.	0.3m^2
Ground station	Gaussian noise standard dev.	1m
SOOP sources	Gaussian noise standard dev.	3m
Closed-loop Doppler (DSRC)	Doppler noise standard dev.	110Hz

TABLE II
MEASUREMENT BIASES CAUSED BY NLOS AND MULTIPATH

Observation	Description	% of bias observations
GNSS pseudorange	Pseudorange biases, 5m~10m	23.57%
UWB ranging	Ranging biases, -5m~5m, 60% of biases lower than 1m	21.62%
SOOP ranging	Ranging biases, 0m~2m	23.49%

can be considered as a zero-mean Gaussian distribution with standard deviation of 110 Hz. In case of SOOP, reference [42] compared the ranging performance of several SOOP signals, where the accuracy of digital television signal can reach 3 m. The standard deviation of ground station ranging errors is set to 1 m based on the empirical value. Detailed sensor configuration and parameters used in simulation are listed in Table I.

To simulate realistic scenarios which also consist of abnormal cases where signals experience NLOS and multipath distortions, measurement biases (i.e. non-zero error means) are simulated to GNSS pseudorange, UWB and SOOP signals. For GNSS pseudorange, signal multipath and NLOS will lead to the code delay tracking [43], so that the code and carrier tracking accuracy will be degraded, here we assume that each GNSS receiver has an integrity method such as [44] or [45] to detect and remove pseudorange measurements with large biases. However integrity methods cannot remove small magnitude of biases, thus we simulate the amplitude remaining pseudorange measurement biases as 5 m~10 m. For the UWB NLOS ranging case, [46] proposed an identification and mitigation method to deal with the NLOS signal, so the biases after mitigation are between −5 m~5 m, and 60% of biases are lower than 1 m. Referring to the NLOS bias of the TDOA SOOP signal, we simulate the TDOA NLOS biases according to the experimental results in [47] where most of the NLOS errors are 0 m~2 m. All the simulated biases are listed in Table II.

In the simulation, there is randomness in the number of visible satellites for each vehicle and the occurrence of multipath and NLOS. The tag '% of bias observations' in Table II means the average percentage of bias observations compared to all the observations in each simulation trials. The position of satellites in view are listed in Table III, the average satellite visibility for all vehicles during 200 simulation trials are showed in Fig. 6.

TABLE III
SATELLITE POSITION IN ECEF FRAME

Satellite	x(m)	y(m)	z(m)
1	19263524	-13725770	11583188
2	26124976	-5749420	-846377
3	24768710	1601307	9925575
4	8048029	-13014437	21563572
5	8543818	15561017	19676844
6	2082386	23437415	12048145
7	22196864	1794375	8737592
8	5129417	-15896254	19534786
9	46895257	9753647	6534686
10	24699427	-8676457	88547042
11	18754121	-12156982	13943714
12	7966175	21258467	11597546
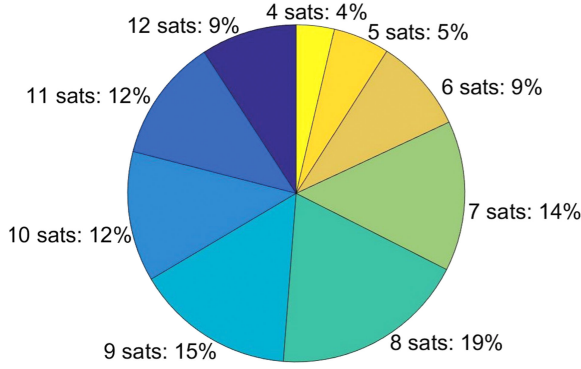
Fig. 6.   Average satellite visibility for all the vehicles during 200 Monte Carlo simulation trials.
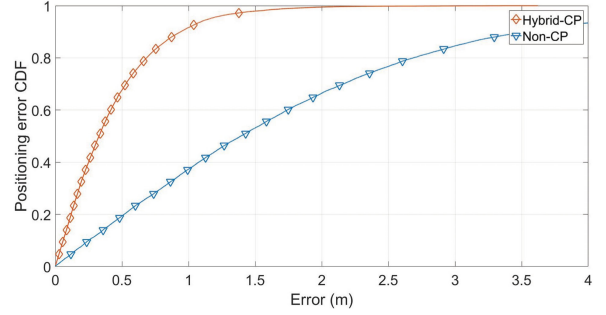

Fig. 7.   CDF Comparison between hybrid-CP and non-CP for all vehicles (positioning errors from 200 simulation trials).

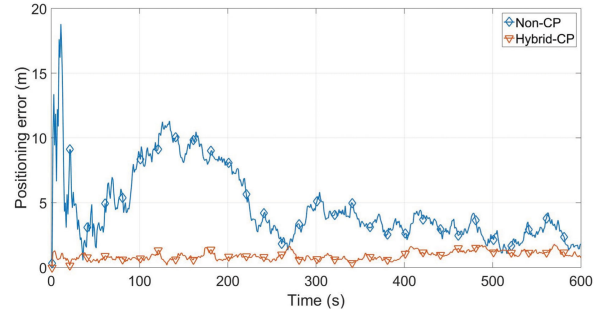Fig. 8.   The example performance of position error for a single vehicle between hybrid-CP and non-CP.

The positioning estimation errors in all simulations are calculated by:

$$E = \sqrt{Err_E^2 + Err_N^2 + Err_U^2} \tag{52}$$

where Err_E, Err_N, Err_U are estimation errors in three directions of east, north and up (ENU) respectively.

B. Comparing Between Non-Cooperative Case and Proposed Hybrid-CP

This parts aims to demonstrate the effectiveness of hybrid-CP. The measurements used in this part are GNSS pseudorange and pseudorange Doppler, UWB ranging and closed-loop Doppler between vehicles. SOOP sources and ground station are not considered. The comparisons are between the proposed Hybrid-CP, and the tightly coupled GNSS/INS integrity system without CP mechanism (Non-CP, details can be found in Chapter 12 of [48]). For the proposed method, the GNSS measurements are the double differenced pseudoranges and pseudorange Doppler between vehicles. However, for the non-CP case, GNSS measurements used in the tightly coupled GNSS/INS are the un-differenced data.

The tightly coupled GNSS/INS system used in non-CP is based on the Kalman filter. Its estimated states, system model and observation model are defined as:

$$\mathbf{X}_{non} = [\phi_e, \phi_n, \phi_u, \delta v_e, \delta v_n, \delta v_u, \delta L, \delta\lambda, \delta h,$$

$$\delta t, \varepsilon_{bx}, \varepsilon_{by}, \varepsilon_{bz}, \varepsilon_{rx}, \varepsilon_{ry}, \varepsilon_{rz}, \nabla_x, \nabla_y, \nabla_z] \tag{53}$$

$$\dot{\mathbf{X}}_{non} = \mathbf{F}_{non}\mathbf{X}_{non} + \mathbf{B}_{non}\mathbf{W}_{non} \tag{54}$$

$$\mathbf{Y}_{non} = \mathbf{H}_{non}\mathbf{X}_{non} + \mathbf{V}_{non} \tag{55}$$

here, the states $\mathbf{X}_{non}$ is similar to the states $\mathbf{X}$ in (25) where the only difference is receiver clock error δt should be estimated, because there is no double differenced data for a single vehicle. $\mathbf{F}_{non}, \mathbf{B}_{non}$ and $\mathbf{W}_{non}$ are the INS system model, noise transfer matrix and system process noise respectively that taking the clock error into consideration. $\mathbf{Y}_{non}$ is the observation vector for pseudorange and pseudorange Doppler observations, $\mathbf{H}_{non}$ and $\mathbf{V}_{non}$ are the corresponding observation matrix and measurement noise.

Based on 200 simulation trials, Fig. 7 gives the simulation results for two cases, cumulative distribution functions (CDF) of estimation errors for all vehicles is used as performance metric. As illustrated, the positioning performance of hybrid-CP has better performance. In non-CP case, GNSS/INS integrated systems are used to provide positioning information, and there is no cooperative relationship between vehicles, thus the positioning accuracy is the lower than CP case. In hybrid-CP case, the proposed method is seen to visibly improve the positioning performance of all vehicles.

To compare the positioning performance under the hybrid-CP and non-CP case more clearly, the example performances of a single vehicle are illustrated in Fig. 8 and Fig. 9, where positioning error and positioning RMSE are used as performance metrics. Due to the effect of urban buildings or other vehicles, the number of visible satellites for the example vehicle is always lower than the total number of satellites in Table II, and
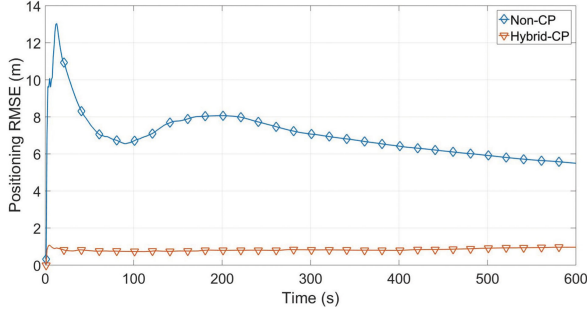
Fig. 9. The example performance of position estimation root mean square error (RMSE) for a single vehicle between hybrid-CP and non-CP.
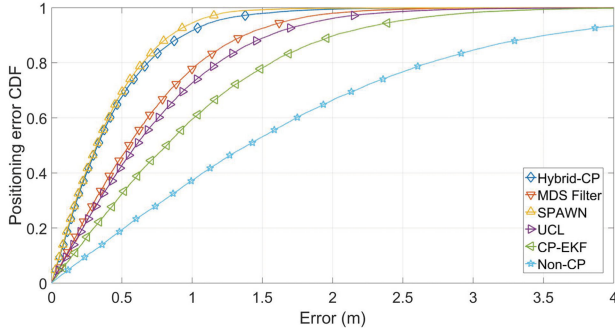

Fig. 10. Positioning error CDF comparisons for all vehicles: hybrid-CP, MDS Filter, SPAWN, UCL, CP-EKF, non-CP (positioning errors from 200 simulation trials).

signal NLOS and multi-path are frequently happened during the trajectory.

Fig. 8 and Fig. 9 show the estimation error comparisons of a single vehicle based on the condition of visible satellites in Fig. 6. In the non-CP case, without the hybrid-CP, the vehicle has the lower positioning accuracy. The positioning performance of a single vehicle largely depends on its visible satellites and the quality of measurements. Due to the relatively fewer number of useful measurements and the existence of multipath and NLOS, non-CP needs more time to converge at the beginning, and has some large amplitude errors during the trajectory. For the hybrid-CP case, under the proposed cooperative mechanism, a single vehicle has a much better positioning accuracy and stability. This is because all the measurements among the collaborators are used in Hybrid-CP processing, and the effect of faulty measurements can be reduced by large numbers of normal measurements.

C. Comparison of Different CP Algorithms

To compare the performance of proposed hybrid-CP with other methods, several CP algorithms are simulated in this section. The available observations for all vehicles are the same as the simulation in *Section B*: GNSS, UWB and closed-loop Doppler. The positioning error CDF of all vehicles is used as the performance metric.

Fig. 10 shows the comparison results among MDS Filter [21], UCL [20], SPAWN [18], Cooperative Extended Kalamn filter

(CP-EKF) [49] and non-CP, where non-CP is adopted as the performance baseline. Here we present the details of each CP algorithm.

1) MDS Filter: The method based on the multidimensional scaling (MDS) and the maximum likelihood estimation. The procedure of MDS Filter is mainly consists of iteration from *step 1* to *step 3*:

step 1: Obtaining the non-cooperative *priori* positioning estimation from a single vehicle, here we use the results $\mathbf{X}_{non}$ of non-CP in (53); *step 2:* Conducting MDS computation based on the stress function in each iteration, using the inter-vehicle UWB and DSRC measurements, until it meets the terminal threshold; *step 3:* Estimating the covariance of CP results, and apply it to a ML filter to make a further estimation.

2) UCL: A universal cooperative localizer using GAMP as the CP estimator, which is similar to the description in *part B, Section III*. However, UCL is not suitable for three-dimensional (3D) positioning, and does not take multiple observations into consideration at each computation epoch. For fairness of comparison, here we adapt it to the 3D positioning case and take various types of observations into consideration.

3) SPAWN: The sum-product algorithm for wireless network. This method is the typical positioning algorithm based on belief propagation that uses the marginal distribution to estimate the navigation states, which is widely considered has superior performance. Its principle is message passing that is same as equations (9) to (12). Here we adopt the importance sampling method in [50] to obtain the marginal distribution. The number of samples is set to 1000.

4) CP-EKF: A cooperative positioning method based on EKF, which fuses the measurements of other collaborators and local data. The estimated states and system model are the same as equations (53) and (54), but take the cooperative measurements from inter-vehicle ranging and Doppler into consideration in the observation model.

Compared to SPAWN, hybrid-CP is a simplified method using linearization during the message passing, which is similar to the difference between particle filter (PF) and extended Kalman filter (EKF). Thus, in Fig. 10, hybrid-CP can achieve comparable and similar performance to SPAWN with much lower computation complexity, where the slight performance loss is caused by the linearization of GAMP. Compared to other methods, hybrid-CP has better accuracy. For example, the probability of errors smaller than 1 m ($P(error < 1\,\mathrm{m})$) is 0.925 for hybrid-CP, but only 0.801, 0.741, and 0.594 for MDS Filter, UCL and CP-EKF respectively. And we find that without the cooperative scheme, the non-CP case has the worst performance due to limited measurements and some measurement biases.

To further analyze the efficiency of hybrid-CP, Fig. 11 compares the computation load of the above methods in one example trial, the processing time for each epoch (processing frequency is 1 Hz) is used as the performance metric. The data are obtained by using Matlab 'tic' and 'toc' functions to record the running time of codes, which can by and large represent the algorithm efficiency.
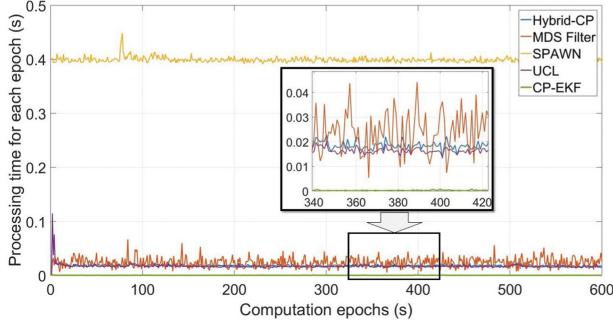
Fig. 11. Example of processing time at each computation epoch: hybrid-CP, MDS Filter, SPAWN, UCL, CP-EKF.

TABLE IV
SIMULATION COMPARISON FOR ALL SIMULATED CASES

	GNSS	UWB	Close-loop Doppler	Ground station	SOOP
Case1	✓	✓	✓		
Case2	✓	✓	✓	✓	
Case3	✓	✓	✓	✓	✓

For hybrid-CP, its computation load derives from the matrix multiplications in GAMP and the Kalman filter. Thus the processing times of hybrid-CP are slightly larger than that of UCL, because UCL just uses GAMP. For the MDS filter, its computation efficiency is similar to the hybrid-CP and UCL but with relatively strong fluctuation. This is mainly because the MDS Filter largely depends on non-cooperative *priori* positioning estimation from a single vehicle, which is affected by measurement biases. Due to the low computation complexity, CP-EKF has the lowest processing time as it is a one-step computation for each epoch that does not involve iteration. For SPAWN, its processing time is about 20 times larger than that of equivalent existing methods, and our proposed method in this scenario of 10 vehicles. It is well-known that the particle filter-based SPAWN cannot scale well with a growing number of vehicles as the number of particles has to grow exponentially with increased dimensionality of the navigation states.

D. Comparison of Hybrid-CP in Case of Different Available Observations and Cooperative Neighbor Nodes

The main benefit of hybrid-CP is the ability to fuse all the possible navigation measurements and estimate the navigation state cooperatively. Therefore this section will firstly evaluate the proposed method in the case of different available observations. The criteria for all cases are summarized in Table IV:

1) Case 1: All vehicles take part in hybrid-CP, using the observations from GNSS, UWB ranging and Close-loop Doppler, but do not use the measurements from the ground station and SOOP sources.

2) Case 2: All vehicles take part in hybrid-CP, and the measurements from the ground station are also used during the estimation.

3) Case 3: All vehicles take part in hybrid-CP, the measurements from the ground station and SOOP sources are used.
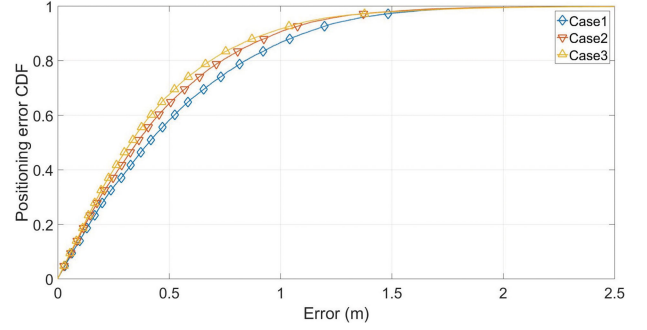

Fig. 12. Hybrid-CP error CDF comparisons for all vehicles in different cases of available observations.
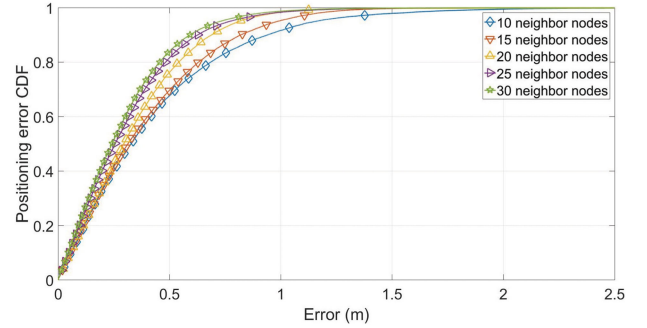

Fig. 13. Positioning error CDF comparisons in different cases of available neighbor nodes: 10, 15, 20, 25, 30.

Fig. 12 gives the performance curves of hybrid-CP in different cases of available observations. As illustrated, the positioning performance improves from *Case 1* to *Case 3*. In *Case 1*, the available observations are GNSS, UWB and Close-loop Doppler, due to the limited navigation observation, its positioning accuracy is obviously lower than *Case 2* and *Case 3*. In *Case 2*, with the supplement measurements from ground stations, its positioning accuracy has a obvious improvement than *Case 1*. And with the increasing types of observations, *Case 3* is more accurate than *Case 2*.

Also, the performance of hybrid-CP should be discussed in cases of different available neighbor nodes. Based on the available observation condition *Case 1* described in Table IV, Fig. 13 shows the performance comparison of hybrid-CP in five cases of available cooperative neighbor nodes: 10, 15, 20, 25 and 30. The hybrid-CP with 30 nodes has the best CP performance, and it is obvious that the estimation accuracy is improving with the number of vehicles. Also, we can find that the cooperative performance gain is decreasing with the growing number of cooperative neighbor nodes. This phenomenon is mainly caused by the decay of the cooperative position error bound [51].

V. CONCLUSION

This paper proposes a hybrid-CP algorithm for vehicular network application, which can fuse various navigation measurements and estimate the navigation states cooperatively. Using generalized approximate message passing (GAMP), the cooperative messages can be approximated by CLT and Taylor

series expansion, and transform the CP problem to a linear mixing problem. The time recurrence of navigation states is conducted through the Kalman filter and onboard INS, which can further improve the accuracy of GAMP and initialize GAMP computation in the next epoch.

Simulation results show that, in the simulated scenario, the proposed method provides obvious accuracy improvement over the non-cooperative case. Its estimation accuracy is better than the traditional CP algorithms such as MDS Fliter, UCL, CP-EKF, and it can obtain comparable performance to SPAWN with much lower computation complexity. Also, the performance of the proposed method improves with additional types of measurements and increasing number of cooperative neighbor nodes (vehicles).

APPENDIX A

The detail derivations of equations in (19)–(21) are demonstrated in this part. Recall the message $\Delta_{f_i \to q_j}^{(k)}$ emitted by factor nodes:

$$\Delta_{f_i \to q_j}^{(k)} = c_\Delta + \log \int p\left(\frac{\tilde{m}_i^{(k)}}{f_i^{(k)}}\right) \prod_{r \neq j} \exp \Delta_{f_i \leftarrow q_r}^{(k)} \quad (56)$$

And the function between navigation states and measurements:

$$f_i^{(k)} \approx \left[\mathbf{A}^{(k)}\mathbf{q}^{(k)} + \mathbf{G}^{(k)}\right]_i$$
$$= a_{i,j}^{(k)} q_j^{(k)} + \sum_{l \neq j} a_{i,l}^{(k)} q_j^{(k)} + [\mathbf{G}^{(k)}]_i \quad (57)$$

According to CLT, the distribution of $f_i^{(k)}$ follows the Gaussian distribution with mean $\mu_{f_j^{(k)}}$ and variance $\tau_{f_j^{(k)}}$:

$$\mu_{f_i^{(k)}} = a_{i,j}^{(k)}\left(q_j^{(k)} - \hat{q}_{f_i \leftarrow q_j}^{(k)}\right)$$
$$+ \sum_l a_{i,l}^{(k)} q_{f_i \leftarrow q_j}^{(k)} + [\mathbf{G}^{(k)}]_i \quad (58)$$

$$\tau_{f_j^{(k)}} = \sum_{l \neq j} a_{i,l}^{(k)2} \tau_{f_i \leftarrow q_j}^{(k)} \quad (59)$$

Note that $a_{i,j}^{(k)}$ is the element of $\mathbf{A}^{(k)}$ at i-th row and j-th column, $\tau_{f_i \leftarrow q_j}^{(k)}$ is the variance of measurement i from neighbor node j. Then message $\Delta_{f_i \to q_j}^{(k)}$ can be further expressed as:

$$\Delta_{f_i \to q_j}^{(k)} = c_\Delta + \log \int \left\{ p\left(\frac{\tilde{m}_i}{f_i^{(k)}}\right) \right.$$
$$\times N\left(f_i^{(k)}; a_{i,j}^{(k)}\left(q_j^{(k)} - \hat{q}_{f_i \leftarrow q_j}^{(k)}\right) + \hat{p}_i^{(k)}, \tau_{i,p}^{(k)}\right) \right\}$$
$$\triangleq c + H\left(\hat{p}_i^{(k)}, \tilde{m}_i, \tau_{i,p}^{(k)}\right) \quad (60)$$

where,

$$\hat{p}_i^{(k)} = \sum_l a_{i,l}^{(k)} q_{f_i \leftarrow q_j}^{(k)} + [\mathbf{G}^{(k)}]_i \quad (61)$$

$$\tau_{i,p}^{(k)} = \sum_l a_{i,l}^{(k)2} \tau_{f_i \leftarrow q_j}^{(k)} \quad (62)$$

Taking the second order Taylor-expansion of message $\Delta_{f_i \to q_j}^{(k)}$ in (58), it becomes:

$$\Delta_{f_i \to q_j}^{(k)} = c_\Delta + \left(\hat{s}_i^{(k)} a_{i,j}^{(k)} + \tau_{i,s}^{(k)} a_{ij}^{(k)2} q_{f_i \leftarrow q_j}^{(k)}\right) q_j^{(k)}$$
$$- \frac{\tau_{i,s}^{(k)2}}{2} a_{i,j}^{(k)} q_j^{(k)2} \quad (63)$$

where, according to the derivation in [36]:

$$\hat{s}_i^{(k)} = \frac{d}{d\hat{p}_i} H\left(\hat{p}_i^{(k)}, \tilde{m}_i, \tau_{i,p}^{(k)}\right)$$
$$= \frac{1}{\tau_{i,p}^{(k)}}\left[E\left(f_i^{(k)} | \hat{p}_i^{(k)}, \tilde{m}_i, \tau_{i,p}^{(k)}\right) - \hat{p}_i^{(k)}\right] \quad (64)$$

$$\tau_{i,s}^{(k)} = -\frac{d^2}{d\hat{p}_i^2} H\left(\hat{p}_i^{(k)}, \tilde{m}_i, \tau_{i,p}^{(k)}\right)$$
$$= \frac{1}{\tau_{i,p}^{(k)}}\left[1 - \frac{\mathrm{var}\left(f_i^{(k)} | \hat{p}_i^{(k)}, \tilde{m}_i, \tau_{i,p}^{(k)}\right)}{\tau_{i,p}^{(k)}}\right] \quad (65)$$

Substituting (63) to (10), the message $\Delta_{f_i \leftarrow q_j}^{(k)}$ emitted by variable node $q_j^{(k)}$ is rewrite as:

$$\Delta_{f_i \leftarrow q_j}^{(k)} = c_\Delta + \log\left[p\left(\frac{q_j^{(k)}}{\mu_j^{(k)}}\right) N\left(q_j^{(k)}; \hat{r}_{f_i \leftarrow q_j}^{(k)}, \tau_{rij}^{(k)}\right)\right] \quad (66)$$

where, $\hat{r}_{f_i \leftarrow q_j}^{(k)}$ and $\tau_{rij}^{(k)}$ are the mean and variance of $\sum_{f_i \neq f_i} \Delta_{f_l \to q_j}^{(k)}$ (see (10)) respectively:

$$\hat{r}_{f_i \leftarrow q_j}^{(k)} = \frac{\sum_{f_n \neq f_i}\left(\hat{s}_n^{(k)} a_{n,j}^{(k)} + \tau_{n,s}^{(k)} a_{n,j}^{(k)2} \hat{q}_{f_n \leftarrow q_j}^{(k)}\right)}{\sum_{f_n \neq f_i}\left(\tau_{i,s}^{(k)} a_{n,j}^{(k)2}\right)} \quad (67)$$

$$\tau_{rij}^{(k)} = \sum_{f_n \neq f_i}\left(\tau_{i,s}^{(k)} a_{n,j}^{(k)2}\right)^{-1} \quad (68)$$

REFERENCES

[1] F. Shen, J. W. Cheong, and A. G. Dempster, "An ultra-wide bandwidth-based range/GPS tight integration approach for relative positioning in vehicular ad hoc networks," *Meas. Sci. Technol.*, vol. 26, no. 4, 2015, Art. no. 045003.

[2] K. Ansari, Y. Feng, and M. Tang, "A runtime integrity monitoring framework for real-time relative positioning systems based on GPS and DSRC," *IEEE Trans. Intell. Transp. Syst.*, vol. 16, no. 2, pp. 980–992, Apr. 2015.

[3] B. Paden, M. Cap, S. Z. Yong, D. Yershov, and E. Frazzoli, "A survey of motion planning and control techniques for self-driving urban vehicles," *IEEE Trans. Intell. Veh.*, vol. 1, no. 1, pp. 33–55, Mar. 2016.

[4] G. De Angelis, G. Baruffa, and S. Cacopardi, "GNSS/cellular hybrid positioning system for mobile users in Urban scenarios," *IEEE Trans. Intell. Transp. Syst.*, vol. 14, no. 1, pp. 313–321, Mar. 2013.

[5] Q. Xu, X. Li, B. Li, X. Song, and Z. Cai, "A reliable hybrid positioning methodology for land vehicles using low-cost sensors," *IEEE Trans. Intell. Transp. Syst.*, vol. 17, no. 3, pp. 834–847, Mar. 2016.

[6] C. Mensing, S. Sand, and A. Dammann, "GNSS positioning in critical scenarios: Hybrid data fusion with communications signals," in *Proc. IEEE Int. Conf. Commun. Workshops*, 2009, no. 2, pp. 1–6.

[7] H. M. Georges, Z. Xiao, and D. Wang, "Hybrid cooperative vehicle positioning using distributed randomized sigma point belief propagation on non-Gaussian noise distribution," *IEEE Sensors J.*, vol. 16, no. 21, pp. 7803–7813, Nov. 2016.

[8] M. A. Caceres, F. Penna, H. Wymeersch, and R. Garello, "Hybrid cooperative positioning based on distributed belief propagation," *IEEE J. Sel. Areas Commun.*, vol. 29, no. 10, pp. 1948–1958, Dec. 2011.

[9] P.-H. Tseng, "Cluster-based networks for cooperative localisation," *IET Radar, Sonar, Navigat.*, vol. 11, no. 4, pp. 605–615, 2016.

[10] R. Zekavat and R. M. Buehrer, *Handbook of Position Location: Theory, Practice and Advances*, vol. 27. Hoboken, NJ, USA: Wiley, 2011.

[11] L. Lin, H. C. So, F. K. Chan, Y. T. Chan, and K. C. Ho, "A new constrained weighted least squares algorithm for TDOA-based localization," *Signal Process.*, vol. 93, no. 11, pp. 2872–2878, 2013.

[12] P. Biswas, T.-C. Lian, T.-C. Wang, and Y. Ye, "Semidefinite programming based algorithms for sensor network localization," *ACM Trans. Sensor Netw.*, vol. 2, no. 2, pp. 188–220, 2006.

[13] S. Srirangarajan, A. Tewfik, and Z. Q. Luo, "Distributed sensor network localization using SOCP relaxation," *IEEE Trans. Wireless Commun.*, vol. 7, no. 12, pp. 4886–4895, Dec. 2008.

[14] B. Li, N. Wu, H. Wang, P. H. Tseng, and J. Kuang, "Gaussian message passing-based cooperative localization on factor graph in wireless networks," in *Proc. IEEE/CIC Int. Conf. Commun.*, 2014, pp. 448–452.

[15] A. T. Irish, J. T. Isaacs, F. Quitin, J. P. Hespanha, and U. Madhow, "Belief propagation based localization and mapping using sparsely sampled GNSS SNR measurements," in *Proc. IEEE Int. Conf. Robot. Autom.*, 2014, pp. 1977–1982.

[16] H. M. Georges, Z. Xiao, and D. Wang, "Hybrid cooperative vehicle positioning using distributed randomized sigma point belief propagation on non-Gaussian noise distribution," *IEEE Sensors J.*, vol. 16, no. 21, pp. 7803–7813, Nov. 2016.

[17] W. Yuan, N. Wu, H. Wang, B. Li, and J. Kuang, "Joint synchronization and localization based on Gaussian belief propagation in sensor networks," in *Proc. IEEE Int. Conf. Commun.*, 2015, pp. 6646–6651.

[18] H. Wymeersch, J. Lien, and M. Z. Win, "Cooperative localization in wireless networks," *Proc. IEEE*, vol. 97, no. 2, pp. 427–450, Feb. 2009.

[19] R. Mendrzik and G. Bauch, "Smart sampling for ultra-wideband nonparametric belief propagation indoor localization," in *Proc. 11th Int. ITG Conf. Syst. Commun. Coding*, 2017, pp. 1–6.

[20] S. Wang, F. Luo, and L. Zhang, "Universal cooperative localizer for WSN with varied types of ranging measurements," *IEEE Signal Process. Lett.*, vol. 24, no. 8, pp. 1223–1227, Aug. 2017.

[21] M. Efatmaneshnik, N. Alam, A. Kealy, and A. G. Dempster, "A fast multidimensional scaling filter for vehicular cooperative positioning," *J. Navigat.*, vol. 65, no. 2, pp. 223–243, 2012.

[22] S. Rangan, "Generalized approximate message passing for estimation with random linear mixing," in *Proc. IEEE Int. Symp. Inf. Theory*, 2011, pp. 2168–2172.

[23] N. Alam, A. T. Balaei, and A. G. Dempster, "Relative positioning enhancement in VANETs: A tight integration approach," *IEEE Trans. Intell. Transp. Syst.*, vol. 14, no. 1, pp. 47–55, Mar. 2013.

[24] K. Yu, K. Wen, Y. Li, S. Zhang, and K. Zhang, "A novel NLOS mitigation algorithm for UWB localization in harsh indoor environments," *IEEE Trans. Veh. Technol.*, vol. 68, no. 1, pp. 686–699, Jan. 2019.

[25] M. Kok, J. D. Hol, and T. B. Schön, "Indoor positioning using ultrawideband and inertial measurements," *IEEE Trans. Veh. Technol.*, vol. 64, no. 4, pp. 1293–1303, Apr. 2015.

[26] J. Wang, Y. Gao, Z. Li, X. Meng, and C. Hancock, "A tightly-coupled GPS/INS/UWB cooperative positioning sensors system supported by v2i communication," *Sensors*, vol. 16, no. 7, 2016, Art. no. 944.

[27] S. Monica and G. Ferrari, "Low-complexity UWB-based collision avoidance system for automated guided vehicles," *ICT Express*, vol. 2, no. 2, pp. 53–56, 2016.

[28] H. Takahara, K. Ohno, and M. Itami, "A study on UWB radar assisted by inter-vehicle communication for safety applications," in *Proc. IEEE Int. Conf. Veh. Electron. Saf.*, 2012, pp. 99–104.

[29] V. Moghtadaiee *et al.*, "System-level considerations for signal-of-opportunity positioning," in *Proc. Int. Symp. GPS/GNSS*, Taipei, Taiwan, 2010, pp. 302–308.

[30] A. Coluccia, F. Ricciato, and G. Ricci, "Positioning based on signals of opportunity," *IEEE Commun. Lett.*, vol. 18, no. 2, pp. 356–359, Feb. 2014.

[31] N. Alam, A. T. Balaei, and A. G. Dempster, "A DSRC doppler-based cooperative positioning enhancement for vehicular networks with GPS availability," *IEEE Trans. Veh. Technol.*, vol. 60, no. 9, pp. 4462–4470, Nov. 2011.

[32] K. A. Hafeez, L. Zhao, B. Ma, and J. W. Mark, "Performance analysis and enhancement of the DSRC for VANET's safety applications," *IEEE Trans. Veh. Technol.*, vol. 62, no. 7, pp. 3069–3083, Sep. 2013.

[33] W. Smith and D. Cox, "A closed-loop Doppler measurement for velocity estimation in mobile, multipath environments," in *Proc. IEEE Antennas Propag. Soc. Symp.*, 2004, vol. 3, pp. 2203–2206.

[34] R. Wang, Z. Xiong, J. Liu, J. Xu, and L. Shi, "Chi-square and SPRT combined fault detection for multisensor navigation," *IEEE Trans. Aerosp. Electron. Syst.*, vol. 52, no. 3, pp. 1352–1365, Jun. 2016.

[35] F. Luo, S. Wang, Y. Gong, X. Jing, and L. Zhang, "Geographical information enhanced cooperative localization in vehicular Ad-Hoc networks," *IEEE Signal Process. Lett.*, vol. 25, no. 4, pp. 556–560, Apr. 2018.

[36] J. T. Parker, "Approximate message passing algorithms for generalized bilinear inference," Ph.D. dissertation, The Ohio State University, Columbus, OH, USA, 2014.

[37] U. Kamilov, S. Rangan, M. Unser, and A. K. Fletcher, "Approximate message passing with consistent parameter estimation and applications to sparse learning," in *Proc. Advances Neural Inf. Process. Syst.*, 2012, pp. 2438–2446.

[38] J. García, J. Munir, K. Roth, and J. A. Nossek, "Channel estimation and data equalization in frequency-selective MIMO systems with one-bit quantization," 2016, *arXiv:1609.04536*.

[39] D. Simon, *Optimal State Estimation: Kalman, H Infinity, and Nonlinear Approaches*. Hoboken, NJ, USA: Wiley, 2006.

[40] D. Jiang, V. Taliwal, A. Meier, W. Holfelder, and R. Herrtwich, "Design of 5.9 GHz DSRC-based vehicular safety communication," *IEEE Wireless Commun.*, vol. 13, no. 5, pp. 36–43, Oct. 2006.

[41] B. W. Parkinson, P. Enge, P. Axelrad, and J. J. Spilker, Jr., *Global Positioning System: Theory and Applications, Volume II*. Washington, DC, USA: AIAA, 1996.

[42] C. Yang, T. Nguyen, and E. Blasch, "Mobile positioning via fusion of mixed signals of opportunity," *IEEE Aerosp. Electron. Syst. Mag.*, vol. 29, no. 4, pp. 34–46, Apr. 2014.

[43] N. Zhu, J. Marais, D. Bétaille, and M. Berbineau, "GNSS position integrity in urban environments: A review of literature," *IEEE Trans. Intell. Transp. Syst.*, vol. 19, no. 9, pp. 2762–2778, Sep. 2018.

[44] Z. Jiang, P. D. Groves, W. Y. Ochieng, S. Feng, C. D. Milner, and P. G. Mattos, "Multi-constellation GNSS multipath mitigation using consistency checking," in *Proc. 24th Int. Tech. Meeting Satell. Division Inst. Navigat.*, 2011, pp. 3889–3902.

[45] N. Zhu, J. Marais, D. Bátaille, and M. Berbineau, "Evaluation and comparison of GNSS navigation algorithms including FDE for urban transport applications," in *Proc. ION ITM*, Monterey, CA, USA, 2017, pp. 51–69.

[46] S. Marano, W. M. Gifford, H. Wymeersch, and M. Z. Win, "NLOS identification and mitigation for localization based on UWB experimental data," *IEEE J. Sel. Areas Commun.*, vol. 28, no. 7, pp. 1026–1035, Sep. 2010.

[47] G. Wang, W. Zhu, and N. Ansari, "Robust TDOA-based localization for IoT via joint source position and NLOS error estimation," *IEEE Internet Things J.*, vol. 6, no. 5, pp. 8529–8541, Oct. 2019.

[48] P. D. Groves, *Principles of GNSS, Inertial, and Multisensor Integrated Navigation Systems*. Norwood, MA, USA: Artech House, 2013.

[49] N. Alam, A. Tabatabaei Balaei, and A. G. Dempster, "A DSRC doppler-based cooperative positioning enhancement for vehicular networks with GPS availability," *IEEE Trans. Veh. Technol.*, vol. 60, no. 9, pp. 4462–4470, Nov. 2011.

[50] E. B. Sudderth, A. T. Ihler, M. Isard, W. T. Freeman, and A. S. Willsky, "Nonparametric belief propagation," *Commun. ACM*, vol. 53, no. 10, pp. 95–103, 2010.

[51] Y. Shen, H. Wymeersch, and M. Z. Win, "Fundamental limits of wideband localization—Part II: Cooperative networks," *IEEE Trans. Inf. Theory*, vol. 56, no. 10, pp. 4981–5000, Oct. 2010.

Jun Xiong received the B.S. degree in network engineering from the Nanjing University of Posts & Telecommunications, Nanjing, China, in 2014, and the M.S. degree in communication and information engineering from the Nanjing University of Aeronautics & Astronautics (NUAA), Nanjing, China, in 2017. He is currently working toward the Ph.D. degree in navigation, guidance and control with the College of Automation Engineering, NUAA, Nanjing, China. He is also a Practicum Student with the Australian Centre for Space Engineering Research, University of New South Wales. His research interests include cooperative navigation and cooperative integrity monitoring.
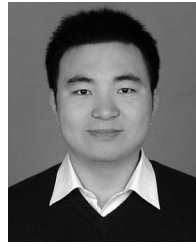
Joon Wayn Cheong (M'18) received the B.Eng. (Hons.) and Ph.D. degrees from the University of New South Wales (UNSW), Sydney, NSW, Australia, in 2008 and 2012, respectively. He is currently a Postdoctoral Research Associate with the School of Electrical Engineering, UNSW. He was the Technical Lead for UNSW's Cubesat mission (named UNSW-EC0) and I-INSPIRE 2, the first two Australian-built Cubesats to become operational in space in 2017. His other research interests in the GNSS field include weak satellite signal acquisition, Assisted-GPS, and non-satellite navigation systems.

Shiwei Tian received the B.S. degree in electronic information engineering from Xidian University, Xi'an, China, in 2008, and the M.S. and Ph.D. degrees in communication and information system from Army Engineering University, PLA, Nanjing, China, in 2011 and 2015, respectively. Since 2015, he has been an Assistant Professor with the College of Communications Engineering, Army Engineering University. His main research interests are satellite navigation, satellite communication, and cooperative positioning.
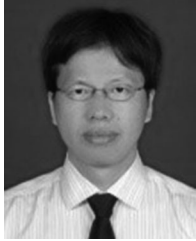
Zhi Xiong received the Ph.D. degree in navigation, guidance and control from the Nanjing University of Aeronautics & Astronautics (NUAA), Nanjing, China, in 2004. He has been with the College of Automation, NUAA, as a Professor. His current research interests include inertial navigation and integrated navigation system.

Rong Wang received the Ph.D. degree from the Nanjing University of Aeronautics and Astronautics, Nanjing, China, in 2014. He is currently with the College of Automation Engineering, Nanjing University of Aeronautics and Astronautics. His research interest includes integrated navigation technology.

Andrew G. Dempster (M'92–SM'03) received the B.E. and M.Eng.Sc. degrees from the University of New South Wales (UNSW), Sydney, NSW, Australia, in 1984 and 1992, respectively, and the Ph.D. degree in efficient circuits for signal processing arithmetic from the University of Cambridge, Cambridge, U.K., in 1995. He is the Director of the Australian Centre for Space Engineering Research, UNSW. He has published in the areas of arithmetic circuits, signal processing, biomedical image processing, satellite navigation, and space systems. He has six patents on new location technologies, and space systems.